

Step meandering: The balance between the potential well and the Ehrlich – Schwoebel barrier

Marta A. Chabowska^{1,*}, Hristina Popova², and Magdalena A. Załuska-Kotur¹

¹*Institute of Physics, Polish Academy of Sciences, al. Lotników 32/46, Warsaw, Poland,*

²*Institute of Physical Chemistry, Bulgarian Academy of Sciences, Acad. G. Bonchev str., 1113 Sofia, Bulgaria*

(Dated: November 20, 2024)

This study presents a comprehensive and innovative exploration of how the surface potential energy landscape influences meander formation. Using the Vicinal Cellular Automaton model, which distinguishes surface diffusion from adatom incorporation into the crystal, the research delves into various factors affecting surface pattern dynamics. By isolating the diffusion process within a defined energy potential, the study provides a detailed analysis of how changes in the potential energy well and the barrier at the top of the step contribute to meander formation. Remarkably, the results reveal that the mere presence of a potential well at the step's bottom is sufficient to induce meandering. The role of the Ehrlich-Schwoebel barrier on already-formed meanders is further investigated, and a mechanism for meander formation is proposed to clarify this process. The derived relation accurately captures the meander length patterns observed in the simulations. Ultimately, the findings demonstrate that the shape of the surface energy potential plays a pivotal role in determining surface pattern formation.

I. INTRODUCTION

Surface morphology and its evolution during crystal growth are crucial in the fabrication of electronic and optoelectronic devices. Achieving control over surface growth to obtain a desired surface pattern is a key goal. However, this control is challenging due to surface instability, as even small energy barriers can have significant effects. One of the primary instabilities is step meandering, a morphological instability driven by surface diffusion. Step meandering has been observed in experiments [1–6] and explored theoretically in numerous studies [7–12]. In general, previous studies have shown that meanders develop with a fixed wavelength and unbounded amplitude during the growth process.

Understanding the mechanism behind step meander formation is crucial from both theoretical and experimental perspectives. It is well established that the Ehrlich–Schwoebel (ES) barrier plays a significant role in the formation of meanders during growth [13, 14]. The ES barrier is an additional diffusion barrier that adatoms encounter when attempting to cross down steps. The formation of step meandering, studied using the kinetic Monte Carlo method, has been linked to the presence of this barrier in the system, along with factors such as temperature and particle flux [10], as well as nucleation processes [11]. Additionally, the wavelength of meanders has been found to depend on the strength of next-nearest-neighbor interactions which influences the relationship between wavelength and deposition rate [12]. The development of meanders has also been investigated through the analysis of a highly nonlinear evolution equation [15–17], revealing that elastic step interactions induce lateral coarsening. Moreover, in Ref. [18], the authors presented an analysis that includes the ES barrier and demonstrates

how the meander wavelength is related to effective step stiffness and adatom mobility, which are strongly influenced by kink concentration. The correlation between kinks and meander instability in the presence of the ES barrier was further confirmed in Ref. [19].

The results obtained by Toru Akiyama and co-authors based on *ab-initio* calculations [20–23] are of particular significance for our analysis. They investigated the stability of the vicinal surface of GaN and AlN, as well as the influence of step edges on the adsorption behavior of particles on such surfaces. Their calculations demonstrate that particles diffusing on a vicinal surface experience a varying surface potential depending on their position on the surface. Notably, it has been demonstrated that there is a potential well at the bottom of the step.

In this paper, we present studies on the formation of meanders and propose an explanation for their formation in the absence of the Ehrlich – Schwoebel barrier. Our approach is based on considering the surface from the perspective of the potential at the surface and afterward examining the effect of this potential on the surface morphology. We further investigate the influence of the presence of the Ehrlich – Schwoebel barrier on meanders formation. The model used here is based on a new approach to the previously introduced $(2 + 1)$ D vicinal Cellular Automaton (VicCA) model [24, 25]. Our findings demonstrate that the ratio of adatom attachment at the kink position to that at the step is a critical factor in the formation of meanders at the surface, particularly in the presence of a potential well at the bottom of the step.

II. THE MODEL

Our model, a new approach to $(2 + 1)$ D vicinal Cellular Automaton model, simulates the evolution of a crystal surface and the diffusion of adatoms on it. Previous studies have explored this model in $(1 + 1)$ D [27–32] and

* galicka@ifpan.edu.pl

(2 + 1)D [24–26] context. The model combines a Cellular Automaton (CA) module for surface growth and a Monte Carlo (MC) module for adatoms diffusion. The CA module updates the surface in parallel based on pre-defined rules, while the MC module simulates adatoms diffusion sequentially.

In the model we assume that one diffusional step is completed when each adatom has been visited on average once. The simulation time step consists of diffusion of adatoms along the surface, surface growth updated within CA module and compensation of the adatoms to their initial concentration c_0 . This approach allows for large-scale simulations. Between two growth modules, all adatoms try n_{DS} diffusional jumps, but only those that point to neighboring unoccupied lattice site are performed. As n_{DS} grows, the growth mode changes from diffusion-limited (DL) to kinetics-limited (KL), and at the same time the transparency of the step increases.

The model uses a square lattice to describe the system and includes two parts - the surface of crystal and the layer of adatoms. The surface typically consists of steps descending from left to right, with the initial distance between them being l_0 . Periodic boundary conditions are applied along the steps, while helical periodic boundary conditions are applied across the steps to maintain the height differences. The incorporation of adatoms into the crystal is governed by CA rules. Three distinct scenarios have been identified in which an adatom becomes part of the crystal structure. The most common locations where an adatom attaches to a crystal and is immediately incorporated are the kinks that are present at the corners of the step. This attachment is determined by the probability, designated as P_k . In the second scenario, an adatom situated in close contact with both a straight step and another adatom becomes a potential crystal site. This incorporation occurs with a probability of P_s . These rules determine the stiffness of the step. We assumed that particles are easily built in the crystal at kinks, and more difficult at the straight part of the step. The step stiffness can be regulated by increasing or decreasing the probability of the second event. The stiffness of the step is increased when it is more difficult to incorporate adatoms into a straight step. A third situation in which the adatom becomes part of the crystal layer is also possible; in this case, the adatom becomes the nucleus of the new layer regardless of the position of the step. This occurs when at least four adatoms stick together on the terrace. More details about the model can be found in Ref. [24].

The most significant aspect of the model refers to the diffusion of adatoms which serves as the driving force behind the formation of surface patterns. The diffusion process is critically dependent on the energy potential landscape experienced by the atoms. Based on the knowledge derived from the *ab-initio* results [22] we postulate the presence of a potential well (Figure 1a,b) at the bottom of the step, along its. It was assumed that the depth of the potential well remains constant throughout the duration of the simulation, equal to βE_V , where E_V represents the

energy associated with the potential well, $\beta = 1/k_B T$ with T denoting temperature and k_B representing the Boltzmann constant. However, the shape of the surface potential is influenced by a number of different factors, including the presence of dangling bonds, surface reconstruction, and the existence of additional barriers. From the perspective of meander analysis, the previously mentioned Ehrlich – Schwoebel barrier at the top of the step is of particular significance. In the event that such a barrier is present, the shape of the potential in our model assumes the form depicted in Figure 1c. The presence of this barrier makes it more challenging for particles to execute jumps across the step. The height of this barrier is designated as βE_{ES} . In the model, it is assumed that each particle diffuses independently. All jumps along terraces, with the exception of those in the immediate vicinity of the step, are performed with the same probability, which is equal to 1 after the equal choice of jump direction. The probability of a jump out of the well is equal to

$$P = e^{-\beta E_V}, \quad (1)$$

whereas in the presence of an ES barrier, this probability of a jump across the steps is set to

$$P = \exp(-(\beta E_{ES} + \beta E_V)). \quad (2)$$

The potential well plays a role in localizing particles, resulting in an increase in particle density at the bottom of the step.

III. RESULTS AND DISCUSSION

The primary objective of this paper is to present a clear and simple mechanism for the formation of meanders during the initial stages of their development, both in the absence and presence of the Ehrlich–Schwoebel barrier. In light of the findings pertaining to the surface potential of diffusing adatoms on crystalline surfaces [20–23], we investigated the diverse forms of surface potential and their impact on the formation of the final surface pattern. Furthermore, our aim is to demonstrate which structural behaviors are attributable to the various components of the surface potential. Our investigations were conducted for varying depths of the applied surface potential well and height of the Ehrlich – Schwoebel barrier, if present. The resulting patterns demonstrated stability throughout the process, predominantly assuming a wave-like configuration, namely meanders.

A. Potential well

The study of meanders begins with an analysis of the influence of the depth of the surface potential well on the formation of meanders in the absence of an Ehrlich – Schwoebel barrier. The depth of the potential well, βE_V , was considered within a range of 0.0 to 8.0. This corresponds to the probability of a particle jumping out of

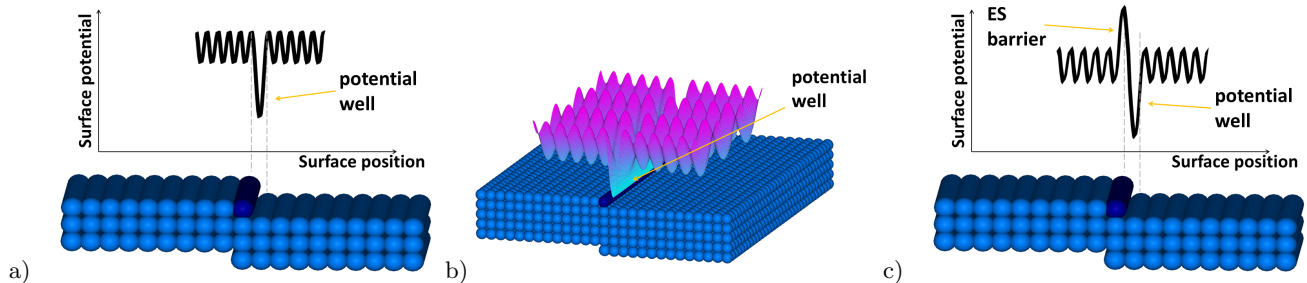


FIG. 1. Visualization of the potential well at the bottom of the step. View from a) the side, b) the top at an angle, c) the side with the additional Ehrlich – Schwoebel barrier.

the well, ranging from 1 (the jump will occur) to $3 \cdot 10^{-4}$ (the jump is less likely to occur). Factor $\beta E_V = 8.0$ means that at temperature of about $700 K$ the energy is $0.48 eV$. The results obtained after 10^6 VicCA simulation time steps are presented in Figure 2 for selected values of βE_V : 0.0, 2.0, 3.5 and 6.0. Initially, the result concerning the scenario without a potential well are presented (Figure 2a). In this case, the final surface configuration exhibits a regular step-like ordering. The introduction of a potential well at the bottom of the step results in the emergence of meanders with a wavelength λ (Figure 2b). An increase in the depth of the potential results in a reduction in the wavelength of the meanders, as illustrated in Figures 2c and 2d. From a certain depth of the potential well ($\beta E_V \approx 5.5$), the wavelength λ does not decrease with the further increasing of the depth of potential well. This can be explained by the fact that the density of particles at step does not increase any more even if potential well is deeper. Additionally, it was verified that the meanders wavelength does not depend on the system size.

B. The Ehrlich – Schwoebel barrier

The formation of meanders is typically attributed to the existence of an Ehrlich – Schwoebel barrier at the top of the step. Consequently, we proceeded to assess the influence of this barrier as a subsequent step of our investigation. The ES height we examined within the range of 0.0 to 8.5, which corresponds to energy in the range of 0.0 eV to 0.51 eV, assuming a growth temperature of around $700 K$. Now the probability of jump across the step and out of the well is in the range from 1 to $7 \cdot 10^{-8}$. The results obtained for values equal to βE_{ES} : 2.0, 4.0, 6.0 and 8.0 in the absence of the potential well are presented in Figure 3. The introduction of the Schwoebel barrier into the system also results in the formation of meandering steps. However, the morphology of these meanders differs significantly from those observed in the presence of the potential well. The wavelength is considerably longer, and the curvature is significantly smaller. Additionally, the formed canyons between meanders are observed to be deeper. As in the previous case, increasing the height of the ES barrier leads to a

shortening of the wavelength.

C. Mutual correlation between the potential well and the Ehrlich – Schwoebel barrier

The present study demonstrates that the mere presence of a potential well at the bottom of the step is sufficient to cause the formation of meanders at the surface. Additionally, it has been verified that the ES barrier also results in meandering of the step, although the final shape differs. The following step involved an examination of the mutual correlation between the potential well and the Ehrlich – Schwoebel barrier. The initial surface potential is now of the form illustrated in Figure 1c. As expected, the introduction of the Ehrlich – Schwoebel barrier into a system containing an existing potential well resulted in a significant modification of the final patterns, with a notable intensification of the meanders, as illustrated in Figure 4. An increase in the height of the ES results in a reduction in wavelength, and simultaneously to the formation of more meandering final structures. The presence of the ES also induces meandering of steps for the lower values of potential well. The additional barrier causes the canyons formed between the meanders to become deeper than without the barrier, but when βE_V is very large the canyons become shallower again. Additionally, as the depth of the potential well increases, the final structures become less ordered resembling surface roughening.

On the other side, meandered structure can also be influenced by the diffusion rate which in our model we can control by adjusting the number of diffusion jumps n_{DS} . So as a further step, we examined the dependence of the meanders on the diffusion rate and the obtained results are shown in the Figure 5. A comparison of the morphologies obtained for different values of n_{DS} clearly shows that increasing the diffusion rate leads to an increase in the wavelength of the meander.

D. Realistic potentials

To validate our model, we decided to use in the simulations the realistic surface potentials which simultane-

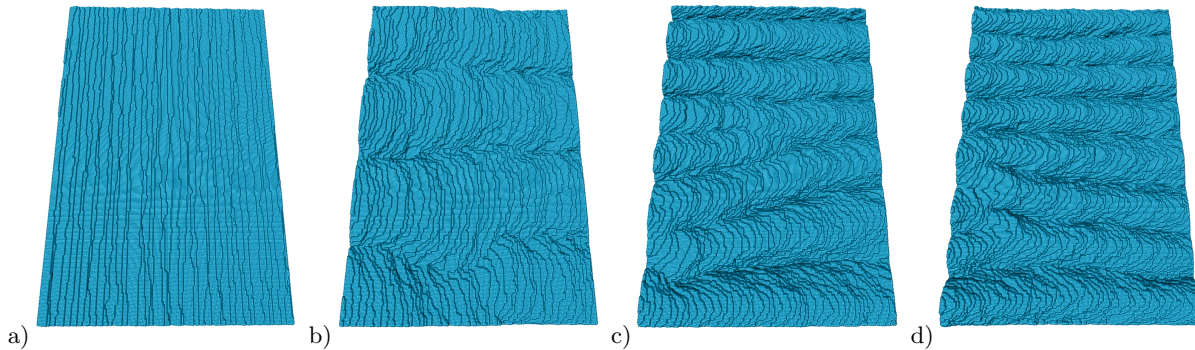


FIG. 2. Meanders obtained for $c_0 = 0.003$, $l_0 = 5$, $n_{DS} = 5$ and a) $\beta E_V = 0.0$, b) $\beta E_V = 2.0$, c) $\beta E_V = 3.5$, d) $\beta E_V = 6.0$, simulation time $t = 2 \cdot 10^6$. System size 200×300 .

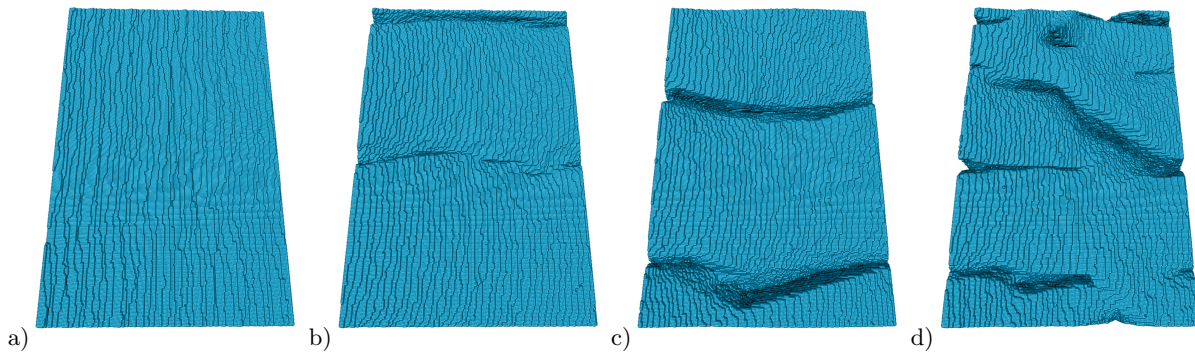


FIG. 3. Meanders obtained for $c_0 = 0.005$, $l_0 = 5$, $n_{DS} = 5$, $\beta E_V = 0.0$ and a) $\beta E_{ES} = 2.0$, b) $\beta E_{ES} = 4.0$, c) $\beta E_{ES} = 6.0$, d) $\beta E_{ES} = 8.0$, simulation time $t = 2 \cdot 10^6$. System size 200×300 .

ously could be easily incorporated into our model. To achieve this, we used the energy potential derived from *ab-initio* calculations performed by T. Akiyama and co-workers (Ref. [22]). It is, however, widely recognized that the energies obtained through density functional theory (DFT) calculations are considerably larger than their actual values. Accordingly, rather than employing the precise values of the energies, we applied the mutual relation between the energies. In particular, our attention was directed towards the most distinctive elements in potential landscape, namely the potential wells and the Ehrlich – Schwoebel barrier, as observed in their calculations.

By adapting the aforementioned landscape to our model, we were able to determine the relations between the energy barriers, specifically how high the Ehrlich – Schwoebel barrier is in comparison to the value of the potential well. This procedure leads to the following dependencies: $\beta E_{ES} \approx 0.31\beta E_V$, $\beta E_{ES} \approx 3.67\beta E_V$, $\beta E_{ES} \approx 0.27\beta E_V$ and $\beta E_{ES} \approx 1.67\beta E_V$. These values are taken from Figures 3a, 3b, 4a, and 4b in Ref. [22], respectively. Assuming a potential well depth of $\beta E_V = 2.0$, the height of the ES barrier is equal to $\beta E_{ES} = 0.62, 7.32, 0.54$ and 3.42 , respectively. The resulting morphologies from our simulations with these values are illustrated in Figure 6. In experiments, during the epitaxial growth of GaN by metal–organic vapor phase epitaxy (MOVPE), meanders are observed at temperature 1150 K [6]. At this temper-

ature, assumed above value of the potential well corresponds to the energy equal to 0.25 eV and values of the Ehrlich – Schwoebel barrier to energies equal to 0.08 eV, 0.9 eV, 0.07 eV, 0.42 eV, respectively. It can be seen that the presented results reproduce qualitatively the meanders observed experimentally [1–6].

E. Wavelength diagram

Further, to analyze quantitatively the obtained meandered structures, we measure the wavelength of meanders by means of height-height correlation function $C(r) = C(r_i - r_j) = \langle [h(r_i) - h(r_j)]^2 \rangle$ which describes the average height difference between any two points i and j on the surface separated by distance $r = r_i - r_j$. In addition, the correlation function can be calculated along x and y axis separately, and in this study we are interested in its calculation along y axis which is the direction along steps in which the meanders develop. Thus, in the case of a regular and ordered meander structure, this correlation function exhibits oscillatory behavior, repeating itself regularly at a distance equal to the meander wavelength. Such behavior we observe in our meandered surface morphologies and their characteristic wavelength is measured as the position of the first minimum of the corresponding correlation function.

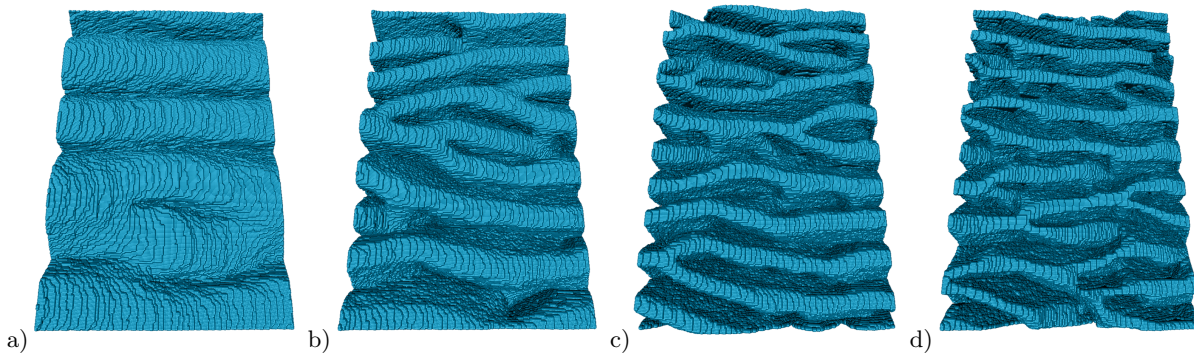


FIG. 4. Meanders obtained for $c_0 = 0.003$, $l_0 = 5$, $n_{DS} = 5$, $\beta_{EV} = 2.0$ and a) $\beta_{ES} = 1.0$, b) $\beta_{ES} = 3.0$, c) $\beta_{ES} = 5.0$, d) $\beta_{ES} = 8.5$, simulation time $t = 2 \cdot 10^6$. System size 200×300 .

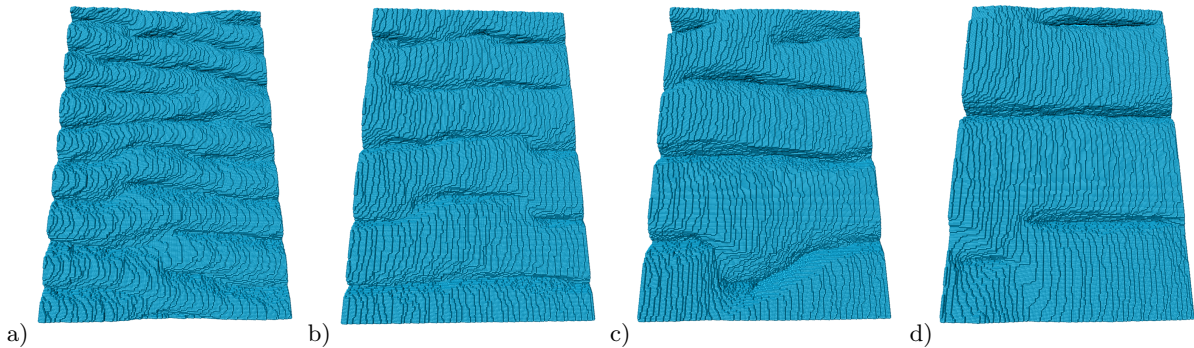


FIG. 5. Meanders obtained for $c_0 = 0.003$, $l_0 = 5$, $\beta_{EV} = 1.0$, $\beta_{ES} = 3.0$ and a) $n_{DS} = 1$, b) $n_{DS} = 2$, c) $n_{DS} = 5$, d) $n_{DS} = 10$, simulation time $t = 2 \cdot 10^6$. System size 200×300 .

Based on this analysis, we perform a systematic study of the meander wavelength λ measured quantitatively for morphologies resulting at different values of the potential well and Schwoebel barrier and investigate in detail the mutual correlation between both of them. The results for λ obtained from our simulation data and averaged over 10 simulation runs are presented in Figure 7. This colored diagram, illustrating the dependence of the meander wavelengths as a function of the depth of the potential well and the height of the Schwoebel barrier, appears as a very useful and informative to determine the potential regions where meanders of proper wavelength can develop. As one can see, at zero potential well and zero Schwoebel barrier meanders do not emerge. For non-zero barriers, the steps start to meander, leading to increasingly shorter wavelengths as the depth of potential well increases. The same behavior can be observed if the Schwoebel barrier becomes higher. The combination of both energies causes an even more dramatic reduction in the meander wavelength. The presented on this diagram isolines, corresponding to values of λ between 25 and 40, define the potential region where well-formed meanders can be obtained. In the bright region above the isoline $\lambda = 25$, when both energies (potential well and Schwoebel barrier) are too high, ordered meanders cannot develop; only an early stage of meandering (or no meandering) is observed and the surface remains rough.

F. The mechanism of meander formation

To elucidate the mechanism of meander formation, it is clear that kinks play a pivotal role [18, 19]. The vicinal cellular automaton model allows us to influence the concentration of kinks by controlling the process of their creation. This process begins with an initially straight step (Figure 8a-1). An adatom diffusing on the surface then reaches the step and attaches to it with a certain probability, denoted as P_s (Figure 8a-2). This attachment automatically generates two kinks that migrate in opposite directions (Figure 8a-3) due to the adsorption of adatoms at the kinks with probability P_k . In the model, we assume that an adatom reaching a kink is always incorporated into the crystal. As a result, both kinks move with a velocity proportional to P_k . Then, another diffusing adatom reaches the newly formed straight step and attaches to it (Figure 8a-4) with probability P_s . Thus, approximately time between first and the second attachment to the step is equal to P_s^{-1} . This means that the meander starts to form after the kinks have moved along the distance

$$\lambda = \frac{P_k}{P_s}, \quad (3)$$

that is approximately equal to a meander wavelength λ . Note, that we can estimate the wavelength of meander

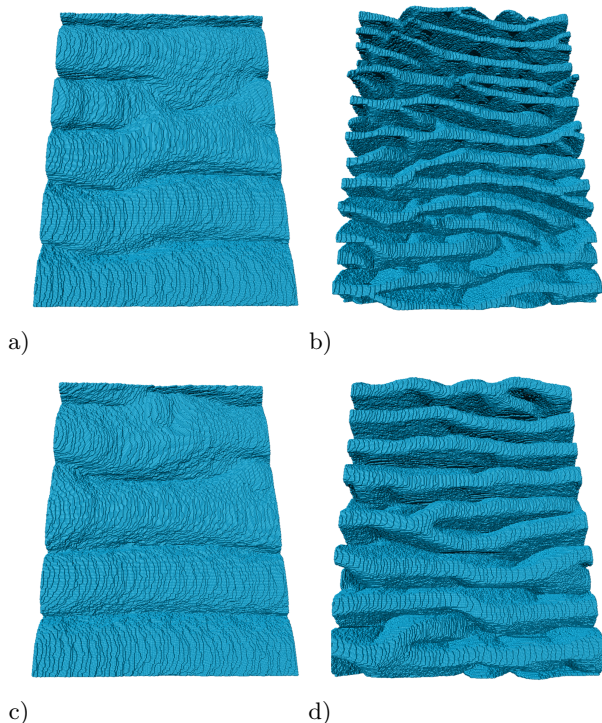


FIG. 6. Meanders obtained for $c_0 = 0.003$, $l_0 = 5$, $n_{DS} = 5$, $\beta E_V = 2.0$ and a) $\beta E_{ES} = 0.62$, b) $\beta E_{ES} = 7.32$, c) $\beta E_{ES} = 0.54$, d) $\beta E_{ES} = 3.42$, simulation time $t = 2 \cdot 10^6$. System size 300×400 . Relations between values of βE_V and βE_{ES} are taken from Ref. [22].

in such a way, but we do not prejudge if meanders would appear at all.

The presence of a Schwoebel barrier on the top of the step results in diffusional screening, which prevents adatoms from reaching the kinks (Figure 8b-4). In this case, the step movement gets faster in the central part of meander and rather slower away from this region due to the limited number of adatoms arriving at these distant locations. As a consequence, the resulting meanders are narrower and exhibit greater curvature, whereas large and deep canyons are formed between them. Such mechanism of meander formation is observed in the presence of Schwoebel barrier, as demonstrated in Figures 3 and 4 for high values of βE_{ES} .

Let us estimate the probability of incorporation. As mentioned earlier, an adatom is incorporated into the crystal at step only if it has another adatom in its immediate vicinity, as illustrated in Figure 8c. Thus, we can calculate the probability P_s as equal to ρ_s^2 . We approximate the density ρ_s , defined as a local particle density at step, by its equilibrium value, assuming that attraction to the step is so slow, that allows for establishing equilibrium. Thus, we have

$$(e^{-\beta E_{ES}} + 1)\rho_l + 2\rho_s = (e^{-\beta E_{ES}} e^{-\beta E_V} + e^{-\beta E_V} + 2 + \frac{\rho_s}{n_{DS}})\rho_s \quad (4)$$

what records balance of streams coming in and out the

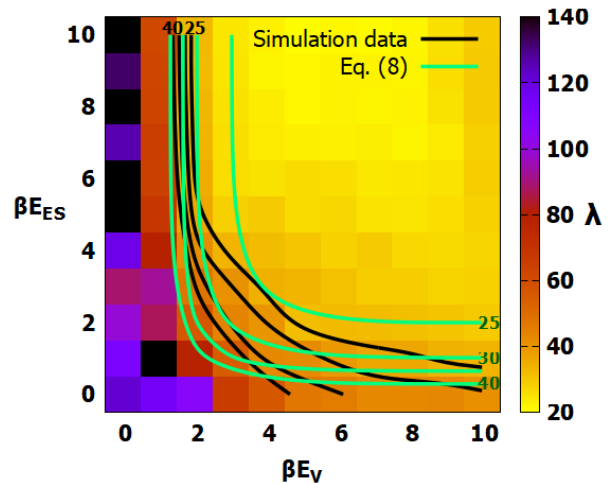


FIG. 7. Diagram of meander wavelength λ as a function of the depth of the potential well βE_V and the height of the Ehrlich – Schwoebel barrier βE_{ES} obtained for $c_0 = 0.003$, $l_0 = 5$, $n_{DS} = 5$ and $t = 2 \cdot 10^6$. Different colors correspond to different meander wavelength. The presented isolines correspond to $\lambda = 25, 30, 35, 40$ and are extracted from simulation data and Eq. (8) respectively.

site at step and where ρ_l is a local particle density at terrace. To complete this equation a normalization equation should be added. But since the whole process is not equilibrium - adatoms are constantly adsorbed and the process is only quasi-stationary, we do not know exactly what this condition should look like. We assume that

$$\rho_l \alpha + \rho_s = \gamma c_0 \quad (5)$$

denoting the balance between the step surroundings and some of the terrace areas. α and γ are constants that should be adjusted. All together gives

$$\rho_s = \frac{\gamma c_0}{e^{-\beta E_V} \alpha + 1} \quad (6)$$

in the first term of expansion in small c_0 . Now, at kink sites, where the local particle density is defined as ρ_k , we expect far from equilibrium situation, because any adatom that arrives to kink is immediately attached to the crystal. Thus, to calculate probability P_k as equal to ρ_k , we sum up streams of adatoms from all four directions

$$\rho_k = 0.25(\rho_s + \rho_l + 2e^{-\beta E_{ES}} \rho_l). \quad (7)$$

Finally, after approximating that in this case $\rho_s \approx \rho_l$, and fitting the formula to extensive data obtained for various model parameters, we determine the constants α and γ , yielding the expression:

$$\lambda = \frac{\rho_k}{\rho_s^2} = \frac{0.066}{c_0} (1 + e^{-\beta E_{ES}}) (0.25 \sqrt{n_{DS}} l_0 e^{-\beta E_V} + 1). \quad (8)$$

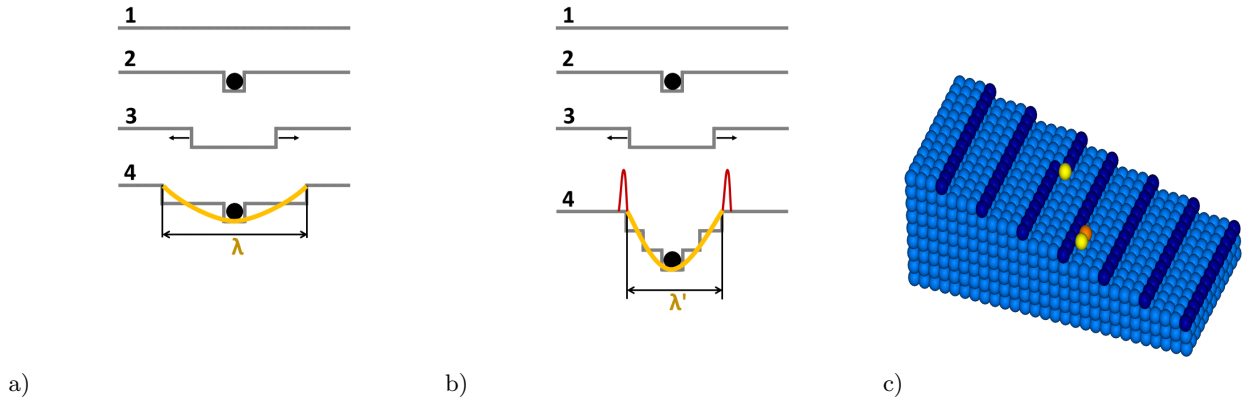


FIG. 8. Visualization of the mechanism of the formation of the meanders a) without, b) with the Ehrlich — Schwoebel barrier present. c) Initial vicinal surface with the adatoms (yellow ball) which become part of the crystal and are involved in the formation of the meanders.

Contours for selected values of meander wavelength, calculated using Eq. 8, are shown in Figure 7. These contours align well with our simulation data. The derived expression provides an approximation; however, as shown in Figure 7, it successfully captures the fundamental relationship between λ , E_V , and E_{ES} . The exponential terms clearly illustrate the independent and combined effects of the potential well and Schwoebel barrier on the wavelength λ , while the prefactors reflect the influence of various model parameters, including c_0 , l_0 , and n_{DS} . A more rigorous and detailed analysis is necessary to fully understand the complexities of the meandering process, which will be a key focus of our future work.

IV. CONCLUSIONS

In this study, we conduct a thorough investigation into the intricate relationship between meander formation and the surface potential energy landscape using the Cellular Automaton model. Our findings highlight the critical role that surface energy potential plays in shaping both the formation and evolution of meanders. One of the most notable discoveries of our analysis is that meanders can form solely due to the presence of a potential well at the bottom of a step, without the need for additional complex conditions. By systematically examining how meander behavior varies with the depth of the potential well, represented by βE_V , we observed a clear trend: as the depth of the potential well increases, the wavelength of the meanders decreases. This observation provides deeper insights into the fundamental mechanisms driving meander formation. Additionally, we examine the influence of the Ehrlich – Schwoebel barrier on meander formation. Interestingly, our analysis

reveals that while meanders can indeed form solely due to the Ehrlich – Schwoebel barrier, their shape is markedly different from those formed by the potential well alone. The balance between the potential well and the Ehrlich – Schwoebel barrier creates meanders with unique characteristics – shorter wavelengths that decrease further as the Schwoebel barrier height increases, resulting in increasingly intricate and complex meander patterns.

To explain this behavior, we propose a mechanism for meander formation. This mechanism suggests that the length of the meanders is determined by the ratio of the probabilities of adatom attachment to kinks and straight steps. Both of these probabilities are functions of local adatom densities. The derived expression successfully captures the observed relationship between meander length and both the Ehrlich – Schwoebel barrier height, βE_{ES} , and the potential well depth, βE_V . These findings not only enhance our understanding of surface pattern formation but also pave the way for further exploration into the dynamics of crystal growth and surface morphology.

ACKNOWLEDGMENTS

The authors thank to Vesselin Tonchev for valuable discussions. Part of the calculations were done on HPC facility Nestum (BG161PO003-1.2.05). The authors thank The Polish National Center for Research and Development (grant no. EIG CONCERT-JAPAN/9/56/AtLv-AlGaN/2023), The Bulgarian National Science Fund (grant No. KP-06-DO02/2/18.05.2023), the Polish Academy of Sciences and the Bulgarian Academy of Sciences (grant No. IC-PL/07/2024-2025) for financial support.

[1] B. Damilano, R. Aristégui, H. Teisseyre, S. Vézian, V. Guigoz, A. Courville, I. Florea, P. Venneguès, M. Bock-

owski, T. Guillet, and M. Vladimirova, Molecular beam epitaxy of GaN/AlGaN quantum wells on bulk GaN sub-

- strate in the step-flow or step meandering regime: Influence on indirect exciton diffusion, *J. Appl. Phys.* **135**, 095702 (2024).
- [2] T.-S. Chou, A. Akhtar, S. Bin Anooz, J. Rehm, O. Ernst, P. Seyidov, A. Fiedler, W. Miller, Z. Galazka, T. Remele, M. Albrecht, and A. Popp, Influencing the morphological stability of MOVPE-grown β -Ga₂O₃ films by O₂/Ga ratio, *Appl. Surf. Sci.* **660**, 159966 (2024).
 - [3] Y.-Z. Wu, B. Liu, Z.-H. Li, T. Tao, Z.-L. Xie, X.-Q. Xiu, P. Chen, D.-J. Chen, H. Lu, Y. Shi, R. Zhang, and Y.-D. Zheng, Homo-epitaxial growth of high crystal quality GaN thin films by plasma assisted-molecular beam epitaxy, *J. Cryst. Growth* **506**, 30–35 (2019).
 - [4] H. Turski, F. Krzyżewski, A. Feduniewicz-Żmuda, P. Wolny, M. Siekacz, G. Muziol, C. Cheze, K. Nowakowski-Szukudlarek, H. G. Xing, D. Jena, M. Załuska-Kotur, and C. Skierbiszewski, Unusual step meandering due to Ehrlich – Schwoebel barrier in GaN epitaxy on the N-polar surface, *Appl. Surf. Sci.* **484**, 771–780 (2019).
 - [5] A. Gocalinska, S. Rubini, and E. Pelucchi, Native oxides formation and surface wettability of epitaxial III–V materials: The case of InP and GaAs, *Appl. Surf. Sci.* **383**, 19–27 (2016).
 - [6] A. Pandey, V. K. Singh, S. Dalal, R. K. Bag, K. Narang, D. Kaur, R. Raman, and R. Tyagi, Effect of two step GaN buffer on the structural and electrical characteristics in AlGaIn/GaN heterostructure, *Vacuum* **178**, 109442 (2020).
 - [7] G. S. Bales, and A. Zangwill, Morphological instability of a terrace edge during step-flow growth, *Phys. Rev. B* **41**, 5500 (1990).
 - [8] O. Pierre-Louis, and C. Misbah, Dynamics and fluctuations during MBE on vicinal surfaces. I. Formalism and results of linear theory, *Phys. Rev. B.* **58**, 2259 (1998); Dynamics and fluctuations during MBE on vicinal surfaces. II. Nonlinear analysis, *Phys. Rev. B.* **58**, 2276 (1998)
 - [9] O. Pierre-Louis, M. R. D’Orsogna, and T. L. Einstein, Edge Diffusion during Growth: The Kink Ehrlich-Schwoebel Effect and Resulting Instabilities, *Phys. Rev. Lett.* **82**, 3661 (1999).
 - [10] M. A. Załuska-Kotur, F. Krzyżewski, and S. Krukowski, Emergence of regular meandered step structure in simulated growth of GaN(0001) surface, *J. Cryst. Growth*, **343**, 138-144 (2012).
 - [11] A. Beausoleil, P. Desjardins, and A. Rochefort, Impact of nucleation on step-meandering instabilities during step-flow growth on vicinal surfaces, *Phys. Rev. E* **89**, 032406 (2014).
 - [12] S. Blel, A. B. H. Hamouda, B. Mahjoub, and T. L. Einstein, Competing growth process induced by next-nearest-neighbor interactions: Effects on meandering wavelength and stiffness, *Phys. Rev. B* **95**, 085404 (2017).
 - [13] G. Ehrlich, and F. G. Hudda, Atomic View of Surface Self-Diffusion: Tungsten on Tungsten, *J. Chem. Phys.* **44**, 1039 (1966); R. L. Schwoebel and E. J. Shipsey, Step Motion on Crystal Surfaces, *J. Appl. Phys.* **37**, 3682-3686 (1966).
 - [14] H.-C. Jeong, and E. D. Williams, Steps on surfaces: experiment and theory, *Surf. Sci. Rep.* **34**, 171-294 (1999).
 - [15] O. Pierre-Louis, C. Misbah, Y. Saito, J. Krug, and P. Politi, New Nonlinear Evolution Equation for Steps during Molecular Beam Epitaxy on Vicinal Surfaces, *Phys. Rev. Lett.* **80**, 4221–4224 (1998).
 - [16] F. Gillet, O. Pierre-Louisa, and C. Misbah, Non-linear evolution of step meander during growth of a vicinal surface with no desorption, *Eur. Phys. J. B* **18**, 519-534 (2000).
 - [17] S. Paulin, F. Gillet, O. Pierre-Louis, and C. Misbah, Unstable Step Meandering with Elastic Interactions, *Phys. Rev. Lett.* **86**, 5538–5541 (2001).
 - [18] A. BH. Hamouda, B. Mahjoub, and S. Blel, Effect of deposition rate and NNN interactions on adatoms mobility in epitaxial growth, *Surf. Sci.* **661**, 42-48 (2017).
 - [19] J. Kallunki, J. Krug, and M. Kotrla, Competing mechanisms for step meandering in unstable growth, *Phys. Rev. B* **65**, 205411 (2002).
 - [20] T. Ohka, T. Akiyama, A. Muizz Pradipto, K. Nakamura, and T. Ito, Effect of Step Edges on Adsorption Behavior for GaN(0001) Surfaces during Metalorganic Vapor Phase Epitaxy: An Ab Initio Study, *Cryst. Growth Des.* **20**, 4358 (2020).
 - [21] T. Akiyama, T. Ohka, K. Nakamura, and T. Ito, Ab initio study for adsorption and desorption behavior at step edges of GaN (0001) surface, *J. Cryst. Growth* **532**, 125410 (2020).
 - [22] T. Akiyama, T. Ohka, K. Nagai, and T. Ito, Effect of step edges on the adsorption behavior on vicinal AlN(0001) surface during metal-organic vapor phase epitaxy: An ab initio study, *J. Cryst. Growth* **571**, 126244 (2021).
 - [23] T. Akiyama, and T. Kawamura, Ab initio study for adsorption behavior on AlN(0001) surface with steps and kinks during metal-organic vapor-phase epitaxy, *Jpn. J. Appl. Phys.* **63**, 02SP71 (2024).
 - [24] M. Załuska-Kotur, H. Popova, and V. Tonchev, Step Bunches, Nanowires and Other Vicinal "Creatures" – Ehrlich – Schwoebel Effect by Cellular Automata, *Crystals* **11**, 1135 (2021).
 - [25] M. A. Chabowska, and M. A. Załuska-Kotur, Diffusion-Dependent Pattern Formation on Crystal Surfaces, *ACS Omega* **8**, 45779-45786 (2023).
 - [26] M. A. Chabowska, and M. A. Załuska-Kotur, Surface Patterns Shaped by Additives in Crystals, submitted to *Vacuum*
 - [27] A. Krasteva, H. Popova, F. Krzyżewski, M. Załuska-Kotur, and V. Tonchev, Unstable vicinal crystal growth from cellular automata, *AIP Conf. Proc.* **1722**, 220014 (2016).
 - [28] F. Krzyżewski, M. Załuska-Kotur, A. Krasteva, H. Popova, and V. Tonchev, Step bunching and macrostep formation in 1D atomistic scale model of unstable vicinal crystal growth, *J. Cryst. Growth* **474**, 135-139 (2017).
 - [29] O. Toktarbaiuly, V. Usov, C. Coileáin, K. Siewierska, S. Krasnikov, E. Norton, S. I. Bozhko, V. N. Semenov, A. N. Chaika, B. E. Murphy, O. Lübben, F. Krzyżewski, M. A. Załuska-Kotur, A. Krasteva, H. Popova, V. Tonchev, and I. V. Shvets, Step bunching with both directions of the current: Vicinal W(110) surfaces versus atomistic-scale model, *Phys. Rev. B* **97**, 035436 (2018).
 - [30] F. Krzyżewski, M. Załuska-Kotur, A. Krasteva, H. Popova, and V. Tonchev, Scaling and Dynamic Stability of Model Vicinal Surfaces, *Cryst. Growth Des.* **19**, 821-831 (2019).
 - [31] H. Popova, F. Krzyżewski, M. A. Załuska-Kotur, and V. Tonchev, Quantifying the Effect of Step-Step Exclusion on Dynamically Unstable Vicinal Surfaces: Step Bunching without Macrostep Formation, *Cryst. Growth Des.* **20**, 7246-7259 (2020).

- [32] H. Popova, Analyzing the Pattern Formation on Vicinal Surfaces in Diffusion-Limited and Kinetics-Limited Growth Regimes: The Effect of Step-Step Exclusion, *Cryst. Growth Des.* **23**, 8875-8888 (2023).